Article

Characterization of Poly(#-caprolactone)-Based Nanocomposites Containing Hydroxytyrosol for Active Food Packaging

Ana Beltran, Artur José Monteiro Valente, Alfonso Jimenez, and María Carmen Garrigós

J. Agric. Food Chem., **Just Accepted Manuscript** • DOI: 10.1021/jf405111a • Publication Date (Web): 19 Feb 2014

Characterization of Poly(ε-caprolactone)-Based Nanocomposites Containing Hydroxytyrosol for Active Food Packaging.

Ana Beltrán[1], Artur J.M. Valente[2], Alfonso Jiménez[1], Mª Carmen Garrigós[1*]

[1]Analytical Chemistry, Nutrition & Food Sciences Department, University of Alicante, 03080, Alicante, Spain, ana.beltran@ua.es, alfjimenez@ua.es, mc.garrigos@ua.es.

[2]Department of Chemistry, University of Coimbra, 3004-535 Coimbra, Portugal

avalente@ci.uc.pt

*All correspondence should be addressed to this author. Tel: +34 965903400. Ext 1242. Fax: +34 965903527. E-mail: mc.garrigos@ua.es

ABSTRACT:

Antioxidant nano-biocomposites based on poly(ε-caprolactone) (PCL) were prepared by incorporating hydroxytyrosol (HT) and a commercial montmorillonite, Cloisite®30B (C30B), at different concentrations. A full structural, thermal, mechanical and functional characterization of the developed nano-biocomposites was carried out. The presence of the nanoclay and HT increased PCL crystallinity, whereas some decrease in thermal stability was observed. TEM analyses corroborated the good dispersion of C30B into the PCL macromolecular structure as already asserted by XRD tests, since no large aggregates were observed. A reduction in oxygen permeability and increase in elastic modulus were obtained for films containing the nanoclay. Finally, the presence of the nanoclay produced a decrease in the HT release from films due to some interaction between HT and C30B. Results proved that these nano-biocomposites can be an interesting and environmentally-friendly alternative for active food packaging applications with antioxidant performance.

KEYWORDS: Poly(ε-caprolactone), Hydroxytyrosol, Nano-biocomposites, Characterization, Active packaging.

INTRODUCTION

Biodegradable and/or bio-based polymers show a number of properties adequate to different applications, including food packaging, automotive, and biomedical fields[1]. Most of these materials have properties comparable to many petroleum-based plastics and are readily biodegradable, making them an attractive potential alternative to reduce the environmental problems induced by the accumulation of plastic waste[2]. Among biodegradable polymers, aliphatic polyesters, such as poly(ε-caprolactone) (PCL), are now commercially available offering an interesting alternative to conventional thermoplastics. PCL can be synthesized either by ring-opening polymerisation (ROP) of the monomer, ε-caprolactone, with a variety of anionic, cationic and coordination catalysts or via free radical ROP of 2-methylene-1-3-dioxepane[3]. PCL is a semicrystalline polymer with a high degree of crystallinity, reaching 69 %[4], but with this value decreasing at higher molar masses. The good solubility of PCL in some common solvents, low melting point (59-64 °C) and exceptional blend-compatibility has raised some interest for the extensive research on potential applications of PCL[3]. However, some drawbacks in using PCL as polymer matrix should be taken into account, particularly its poor thermal and mechanical resistance and limited gas barrier properties. In this sense, PCL commercial uses are currently tempered by its high water solubility, high hydrophilicity, brittleness, low heat distortion temperature, high gas permeability and low melt viscosity[5].

The use of PCL formulations in food packaging applications has been recently evaluated by several authors. In fact, the main current commercial application of PCL is in the manufacture of biodegradable bottles and compostable bags[6]. Martinez-Abad et al. suggested that the combination of cold storage with PCL incorporating ciannamaldehyde, as a natural biocide, could be suitable for the controlled diffusion of

this agent extending the shelf-life of packaged food products[7]. Antimicrobial nanocomposites of PCL with thymol were also developed by Sánchez-García et al[8]. On the other hand, Perez-Masiá et al.[9] used PCL to encapsulate dodecane developing coating materials with energy storage capacity in refrigeration conditions. Blends of chitosan and poly-(ε-caprolactone) for food packaging applications with good tensile strength and low water vapor permeability were studied by Swapna et al.[10], concluding that fruits and vegetables packaged in PCL films were expected to extend their storage life.

In order to improve PCL properties, the incorporation of nanoclays into this matrix is attracting some interest. It is known that the addition of montmorillonites (MMT) in contents lower than 10 wt% to polymer matrices leads to remarkable increases in rigidity (elastic modulus), thermal stability and barrier to gases and vapours[1]. This strategy will be explored in this study to limit the current PCL disadvantages in food packaging applications.

In the last years, several authors have worked on the preparation and characterization of PCL-based nanocomposites[11-13]. Pantoustier et al[14] used the *in-situ* intercalative polymerization method and compared the properties of nanocomposites prepared with both pristine MMT and after modification with amino-dodecanoic acid. Fukushima et al developed nanocomposites of PCL with MMT and sepiolite showing a good dispersion level of clays within the polymer matrix as well as thermomechanical improvement in the resulting nanocomposites[15].

An additional functionality recently proposed for nanocomposites is the controlled release of active substances embedded in food packaging materials[1]. Active packaging is based on the release of specific compounds present in the polymer formulation with controlled kinetics in particular environments[16]. It is known that the addition of active

agents to polymer matrices avoids food degradation processes improving quality, safety and health properties of foodstuff[17]. In this sense, the combination of active technologies, such as the addition of antioxidant and/or antimicrobial agents to packaging materials, with the use of nanocomposites can synergistically lead to formulations with balanced properties and functionalities[8,18]. Regarding the development of active films based on PCL, Salmieri et al[19] incorporated oregano, savory and cinnamon essential oils (EOs) at 1 % (w/w) as natural antioxidants to alginate/PCL-based films. Their results confirmed the plasticizing effect of EOs in addition to their bioactive role, being the oregano-based films the most effective antiradical systems. β-carotene is another widely available natural antioxidant, and it has been reported that the addition of low amounts of this compound to PCL resulted in a significant plasticization of the matrix improving its ductile properties[20]. In this sense, the use of hydroxytyrosol (3,4-dihydroxyphenylethanol, HT), a compound with the highest antioxidant effect amongst the various polyphenols present in olives[21], could be a promising approach from an economical point of view, since it would turn agricultural residues into higher added-value active food packaging additives. In previous studies, certain decrease in thermal properties of natural antioxidants has been observed for compression moulded packaging materials at high temperatures[22]. However, hydroxytyrosol showed a good performance in polypropylene materials acting as antioxidant and it might be considered as a promising alternative to use in active packaging formulations.

The novelty of this work lies on the use of HT as natural antioxidant combined to a commercial nanoclay to develop films for active packaging based on PCL. The addition of the nanoclay could help to improve the intrinsically poor PCL barrier properties. Also, the use of HT is justified to improve shelf-life of foodstuff by the

antioxidant performance of this compound. At the best of our knowledge, there is no evidence in scientific literature of PCL-based packaging systems where the poor thermal resistance and barrier properties of PCL are overcome. In this way, this study is focused on the development and full characterization of new nanocomposites based on PCL, HT and a commercial MMT (Cloisite®30B, C30B), with high potential to improve thermal and barrier properties in biopolymers[23]. Active nano-biocomposite films were obtained by melt-blending followed by compression moulding, which were further characterized on their thermal, structural, mechanical and functional properties. In addition, the release of HT from these nano-biocomposites at different times was also evaluated.

MATERIALS AND METHODS

Materials.

Poly(ε-caprolactone) (PCL, CAPA®6800) commercial grade (pellets) was kindly supplied by Perstorp Holding AB (Sweden). Hydroxytyrosol (98% purity) (HT) was kindly supplied by Fine & Performance Chemicals Ltd (Middlesbrough, UK). The commercial organo-modified montmorillonite used in this study was Cloisite®30B (C30B) and it was supplied by Southern Clay Products (Austin, TX, USA). This nanoclay was synthesized by replacing sodium ions in different silicate layers by methyl bis(2-hydroxyethyl) tallow alkyl ammonium cations by ion exchange.

Nano-biocomposites Preparation.

PCL nanocomposites were processed by melt blending in a Haake Polylab QC mixer (ThermoFischer Scientific, Waltham, MA, USA) at 80 ºC for 5 min at 100 rpm. Before processing, PCL and C30B were left in an oven at 50 ºC for 20 h and 100 ºC for

24 h, respectively, to eliminate moisture. Both additives were introduced in the mixer once the polymer was in the melt state in order to avoid unnecessary losses. The 50 cm^3 mixing chamber was filled with 50 g total mass. Eight different formulations were obtained by adding different amounts of HT and C30B in concentrations ranging 5-10 wt% and 2.5-5 wt%, respectively (Table 1). An additional sample without any additive was also prepared and used as control (PCL0).

Films were obtained by compression-moulding at 120 ºC in a hot-plate hydraulic press Carver Inc, Model 3850 (Wabash, IN, USA). Materials were kept between the plates at atmospheric pressure for 5 min until melting and then they were successively pressed under 2 MPa (1 min), 3 MPa (1 min) and finally 5 MPa (5 min) to liberate the trapped air bubbles. The average thickness of the obtained films was around 200 μm, as measured with a 293 MDC-Lite Digimatic Micrometer (Mitutoyo, Japan) at five random positions (Table 1), after 48 h of conditioning at 50 % relative humidity (RH) and 23 ºC. The final appearance of the films was completely homogenous.

Nano-biocomposites Characterization.

Differential scanning calorimetry (DSC) tests were conducted in triplicate by using a TA DSC Q-2000 instrument (New Castle, DE, USA) under inert N_2 atmosphere. Samples (3 mg) were introduced in aluminium pans (40 μL) and were submitted to the following thermal program: heating from -90 ºC to 160 ºC (3 min hold), cooling to -90 ºC (3 min hold) and heating to 160 ºC, all steps at 10 ºC min^{-1}. The crystallization and melting parameters were determined from the second heating scan. The crystallinity at room temperature (χ_c) of each material was evaluated by using equation (1):

156
$$\chi_c = \left(\frac{\Delta H_m}{\Delta H_m^0 \left(1 - \frac{\%wt_{clay}}{100} \right)} \right) \times 100 \quad (1)$$

157 where ΔH_m is the specific melting enthalpy of the sample and ΔH_m^o is the melting
158 enthalpy of the 100 % crystalline PCL matrix (142.0 J g^{-1})[10].

159 *Thermogravimetric analysis (TGA)* was performed in a TGA/SDTA 851e Mettler
160 Toledo thermal analyzer (Schwarzenbach, Switzerland). Samples (5 mg) were weighed
161 in alumina pans (70 μL) and were heated from 30 ºC to 700 ºC at 10 ºC min^{-1} under N_2
162 atmosphere (flow rate 50 mL min^{-1}). Analyses were repeated three times for each
163 sample.

164 *Tensile tests* were carried out by using a 3340 Series Single Column System
165 Instron Instrument, LR30K model (Fareham Hants, UK) equipped with a 2 kN load cell.
166 Tests were performed in rectangular probes (100 x 10 mm^2), an initial grip separation of
167 60 mm and crosshead speed of 25 mm min^{-1}. Before testing all samples were
168 equilibrated for 48 h at 50 RH %. Tensile strength, elongation at break and elastic
169 modulus were calculated from the resulting stress-strain curves by following the ASTM
170 D882-09 standard[24]. Tests were carried out at room temperature. Five repetitions were
171 performed for each film composition and mean values were reported.

172 *Oxygen transmission rate (OTR)* was determined with an oxygen permeation
173 analyzer (8500 model Systech, Metrotec S.A, Spain). Tests were carried out by
174 introducing O_2 (99.9% purity) into the upper half of the diffusion chamber while N_2 was
175 injected into the lower half, where an oxygen sensor was located. Films were cut into
176 14-cm diameter circles for each formulation and they were clamped in the diffusion
177 chamber at 25 ºC. Tests were performed in triplicate and were expressed as oxygen
178 transmission rate per film thickness (OTR·e).

179 *Scanning electronic microscopy (SEM)* micrographs were obtained for surfaces
180 and cross sections of cryo-fractured films with a JEOL JSM-840 microscope (Peabody,
181 MA, USA) running at 12kV. Samples were coated with gold layers prior to analysis to
182 increase their electrical conductivity. Images were registered at magnifications 100x and
183 500x.

184 *Transmission electron microscopy (TEM)* tests were performed by using a JEOL
185 JEM-2010 microscope (Tokyo, Japan) operated at 100 kV. Films were previously ultra-
186 microtomed to obtain slices of 100 nm thickness (RMC, model MTXL).

187 *X-ray diffraction (XRD)* patterns were recorded at room temperature in the 2.1-40°
188 (2θ) range (step size = 0.01°, scanning rate = 8 s step^{-1}) by using filtered CuK_α radiation
189 (λ = 1.54 Å). A Bruker D8-Advance diffractometer (Millerica, MA, USA) was used to
190 determine the interlayer spacing of clay platelets.

191 *Colour* changes on films surfaces due to the additives were analyzed with a
192 KONICA CM-3600d COLORFLEX-DIFF2 colorimeter, HunterLab, (Reston, VA,
193 USA). The L*, a*, b* system (CIELab) was employed; the L* axis represents the
194 lightness from black (L* = 0) to absolute white (L* = 100), the a* axis varies from
195 green (−) to red (+), and the b* axis varies from blue (−) to yellow (+). These
196 parameters were measured at five different locations on each specimen and average
197 values were calculated. The total colour difference, Δ*E**, between the control PCL film
198 and nanocomposite films was calculated by using equation (2):

199 $$\Delta E^* = \left[\left(\Delta L^* \right)^2 + \left(\Delta a^* \right)^2 + \left(\Delta b^* \right)^2 \right]^{1/2} \qquad (2)$$

200 where Δ*L**, Δ*a** and Δ*b** are the difference between initial and final values (before and
201 after the additives addition) of *L**, *a** and *b**, respectively.

202

203 **HT Release from films.**

The evaluation of the release rate of HT from each film at different times was carried out for 4 cm^2 samples immersed in 100 mL of methanol. The extracts were periodically taken and further analyzed by UV-visible spectroscopy with a Shimadzu Spectrophotometer 2450 (Kyoto, Japan). Spectra were obtained on extracts directly inserted in the cell compartment, and they were studied over the 200-300 nm wavelength range, which includes the maximum absorption wavelength of HT at 281 nm. Spectra were acquired each minute for one hour to ensure that the release of the active agent to the methanol solution had reached a maximum value. In order to quantify the amount of HT released, the specific extinction coefficient, ε (mg^{-1} L cm^{-1}), for HT in methanol was calculated to be 0.0124 mg^{-1} L cm^{-1}, through the measurement of the absorbance *A* at 281 nm of a set of HT standard solutions with concentration, *c* (mg L^{-1}), and by using the Lambert-Beer law equation:

$$A = cl\varepsilon \qquad (3)$$

where l = 1 cm. In all experiments, temperature was kept constant at 25.0 °C with a Multistirrer 6 thermostatic bath from Velp Scientifica (Usmate, Italy). During HT release experiments, composite-containing solutions were stirred at ca. 220 rpm.

Statistical Analysis.

Statistical analysis of results was performed with SPSS commercial software (Chicago, IL, USA). A one-way analysis of variance (ANOVA) was carried out. Differences between average values were assessed on the basis of confidence intervals by using the Tukey test at a $p \leq 0.05$ significance level.

RESULTS AND DISCUSSION

Thermal Characterization.

229 DSC tests were performed to elucidate the effect of the nanoclay and HT addition
230 on the thermal properties of the PCL matrix. Four parameters were determined:
231 crystallization temperature, T_c; melting temperature, T_m; crystallization enthalpy, ΔH_c;
232 and melting enthalpy, ΔH_m. These results are summarized in Table 2. It should be
233 highlighted that the melting temperature of neat PCL was lower than those obtained for
234 the rest of materials formulated in this study. This result gives an indication of the lower
235 crystallinity of neat PCL when compared to nano-biocomposites, as it has been reported
236 by other authors[11].

237 Regarding crystallinity values, this parameter increased with the addition of HT (p
238 < 0.05), due to the interaction between the polymer matrix and the additive molecules,
239 which can show some plasticizing effect. On the other hand, the addition of the polar
240 C30B to the polyester matrix also resulted in a significant increase ($p < 0.05$) of the
241 crystallization rate and could modify the PCL crystalline structure due to the ability of
242 the nanoclay particles to heterogeneously nucleate the crystallization of the polymer
243 matrix, as it has been well documented for a wide range of nanocomposites[25]. Similar
244 results were obtained by Persico et al. in LDPE nanocomposite films containing
245 carvacrol, where differences in crystallinity values were considered a consequence of
246 two main factors: the presence of heterogeneous nucleation sites and changes in chain
247 mobility. In this sense, they reported that clay platelets could act as nuclei for the initial
248 heterogeneous nucleation and subsequent growth of crystallites. Furthermore, they
249 hypothesized that the increase in chain mobility promoted by carvacrol enhanced the
250 ability of the polymer to crystallize[26].

251 However, no significant differences ($p > 0.05$) were observed in crystallinity
252 values for films containing 2.5 and 5 wt% of nanoclay (Table 2). Similar results were
253 found for the ternary nano-biocomposites containing the same amount of C30B ($p >$

254 0.05), and a decrease for those with 5 wt% of nanoclay, although without significant
255 differences ($p > 0.05$). In this sense, it was reported that the variations in the
256 crystallinity by the addition of nanoclays can be accounted for by two factors:
257 nucleation that increases crystallinity and reduction in the flexibility of polymer
258 macromolecular chains that impedes their rearrangement into ordered crystalline
259 structures, reducing crystallinity. Both factors are related to nanoclay dispersion and
260 content and different results should be obtained depending on the prevailing effect[11].
261 Furthermore, the addition of HT enhanced polymer chain mobility promoting its self-
262 nucleation and crystallinity. In conclusion, the neat crystallinity observed for materials
263 with both additives (HT and C30B) can be attributed to the superposition of all these
264 contributions. The reduction in chain mobility as the result of the nanoclay addition can
265 be considered an important factor in controlling the final properties and structure
266 developed by the material.

267 TGA results indicated that the thermal degradation of PCL in inert atmosphere
268 took place through the rupture of the polyester chains via ester pyrolysis reaction with
269 the release of CO_2, H_2O and carboxylic acids. In the case of polyesters, such as PCL,
270 pyrolysis results in chain cleavages randomly distributed along the macromolecular
271 chains. It was reported that when two pyrolysis reactions occur with neighbouring ester
272 functions, 5-hexenoic acid is one of the reaction products[13]. TGA curves obtained for all
273 the studied PCL nano-biocomposites just showed one main degradation step. The initial
274 degradation temperatures (T_{ini}), determined at 5 % weight loss, and maximum
275 degradation temperatures (T_{max}) obtained for all formulations are shown in Table 3. The
276 incorporation of the active compound and the nanoclay brings about a significant effect
277 on the thermal stability of the obtained nano-biocomposites ($p < 0.05$). In this sense, the
278 addition of 10 wt% HT to PCL resulted in 18 ºC reduction in T_{ini}. This result could be

279 explained by the plasticizing effect of HT to PCL, as already stated in the DSC study. In
280 this sense, it was reported that the addition of plasticizers to bio-polyesters, such as
281 PLA, results in some decrease in the polymer thermal stability[27]. On the other hand, the
282 addition of the nanoclay also produced some significant decrease ($p < 0.05$) in the PCL
283 thermal stability, but this decrease was not enough to result in PCL degradation at
284 processing temperatures. It was reported that layered silicates could catalyze PCL
285 pyrolysis by a catalytic action played by the nanoclay due to the presence of Lewis
286 acidic sites, created upon organic modifier degradation[13].
287
288 **Mechanical properties.**
289 The addition of low nanoclays contents (less than 10 wt%) to polymers is
290 expected to improve mechanical properties, particularly when effective nanoclay
291 exfoliation occurs[22,1]. The enhancement in mechanical properties of polymer
292 nanocomposites can be attributed to the high rigidity and aspect ratio of nanoclays
293 together with the good affinity through interfacial interaction between polymer matrix
294 and dispersed nanoclay[28].
295 In this study, tensile tests were performed to evaluate the influence of the addition
296 of the nanoclay and/or the active additive on the mechanical properties of PCL-based
297 nano-biocomposites. Results are shown in Table 3, where the elastic modulus E (MPa),
298 elongation at break ε_B (%) and tensile strength TS (MPa) were determined in all
299 materials. The addition of HT to PCL resulted in some modification in E and ε values (p
300 < 0.05), while no significant differences were observed in TS ($p > 0.05$). In this sense,
301 an increase in the HT concentration caused an increase in ε and a decrease in E values
302 compared to the neat polymer. This behaviour could be explained by the plasticizing
303 effect of HT resulting in the increase in ductility of the polymer and it is consistent with

304 results obtained by other authors with the addition of similar additives to biopolymer
305 matrices[20,29]. In this sense, it should be noted that the physical state of HT is a viscous
306 liquid, with the consequence of the intimate mixture of HT molecules within the
307 macromolecular chains, permitting the enhancement on the internal movement and
308 consequently on ductile properties.

309 On the other hand, the addition of the nanoclay caused a significant increase in
310 both, the elastic modulus and elongation at break of the nano-biocomposites ($p < 0.05$).
311 Concomitantly, a decrease (ca. 40%) of tensile strength ($p < 0.05$) was observed when
312 the amount of the nanoclay in the film increased from zero to 5 wt%. The constrained
313 polymer model developed by Beall can be used to explain some of the general
314 phenomena observed in polymer/clay nanocomposites, including changes in mechanical
315 properties, such as modulus improvement and increased elongation at break. In this
316 sense, the constrained polymer region could be viewed as temporary crosslinks, which
317 certainly contribute to increase moduli but when strained can break and reform as the
318 stress and strain increase. In examining the crazes formed in composites that exhibit this
319 increase in elongation at break it has been observed that fibrils form where the clay
320 plate align along the direction of the fibril length. This gives a convenient platform for
321 the polymer to break the temporary crosslinks and then reattach along the clay
322 platelets[30]. For the ternary nano-biocomposites, and regarding the E values, it was
323 observed that the effect of the nanoclay was predominant for C30B5 ternary composites
324 resulting in a clear increase in E values ($p < 0.05$) while a superposition of the influence
325 of both additives, i.e. nanoclay and HT, should be taken into account to explain results
326 obtained for C30B2.5 materials. In fact, the ultimate behaviour observed in mechanical
327 properties can be considered as the result of several factors, such as crystallinity,
328 polymer plasticization, filler-matrix interface, which affect the stress-strain properties in

329 a complex way[26]. Although the difficulties of considering antagonist effects by HT and
330 C30B in ternary composites, it could be concluded that the addition of the nanoclay
331 induced reinforcement effects provided by the high aspect ratio and surface area of
332 silicate layers. The improvement in these properties could be considered a clear
333 indication of the high dispersion of the nanoclay through the polymer matrix and their
334 high compatibility[31].
335
336 **Morphological study.**
337 SEM micrographs of films (not shown) showed a featureless and non-porous
338 morphology, indicating a good dispersion of C30B and HT in the PCL matrix; ie., no
339 phase separation was observed.
340 The morphological characterization of these materials was completed by
341 transmission electron microscopy (TEM), allowing a qualitative evaluation of the
342 dispersion degree of the nanoclay in the PCL matrix. TEM micrographs of PCL
343 nanocomposites containing C30B showed partial exfoliation, since swollen and single
344 dispersed clay layers were observed (Figure 1). Complete exfoliation of nanoclays into
345 individual platelets is not often achieved in nanocomposites and consequently a mixed
346 morphology consisting of intercalated and exfoliated structures is usually obtained[1].
347 In general terms, TEM tests suggested the good dispersion of C30B in the PCL
348 matrix, since no aggregates were observed. These results could be attributed to the
349 strong interactions between polymer and nanoclay, caused by the hydrogen bonding
350 between the carbonyl group in the polymer structure and the hydroxyl groups of the
351 organo-modified nanoclay[1].
352
353 **XRD analysis.**

354 The dispersion of clays in nanocomposite films was studied by using X-ray
355 diffraction (XRD). The XRD pattern of PCL was characterized by the presence of two
356 distinct peaks at 2θ = 24.9° and 27.5° corresponding to the (110) and (200) planes,
357 respectively suggesting a semi-crystalline structure[14]. No noticeable differences were
358 found from the XRD patterns for all formulations in this angle range, suggesting that the
359 polymer matrix structure was not influenced by the presence of the filler and/or HT.
360 The most important variations in XRD patterns of these PCL-based nano-
361 biocomposites were found in the low angle range (below 10º), which gives indication of
362 the clay dispersion into the polymer matrix (Figure 2). C30B was characterized by a
363 single diffraction peak at 2θ = 4.8°, corresponding to the (001) basal reflection[14],
364 accounting for 18.6 Å interlayer distance. A shift of the clay diffraction peak to lower
365 angles in these nano-biocomposites was observed, indicating a good interaction of the
366 nanoclay with the polymer matrix, showing an increase in the interlayer distance up to
367 32.7 Å for PCL/C30B5 due to the intercalation of PCL macromolecular chains into the
368 clay galleries. Ludueña et al. reported similar results for PCL/C30B nanocomposites
369 showing a final d_{001} spacing value increased to 33.1 Å (79% from the initial value)[32].
370 These results could be also correlated with those obtained for oxygen barrier properties,
371 since an inverse correlation between d-spacing and oxygen transmission rate was
372 apparent[28]. However, there was no shift in the interlayer distance in nano-biocomposites
373 with different clay content, suggesting that clay load did not affect the clay platelets
374 intercalation. Similar results were found by Ahmed et al. for PCL/C30B films with
375 nanoclay compositions ranging from 2.5-10 wt%[12].
376 In addition, some decrease in the C30B peak intensity was observed, in particular
377 when the active additive was introduced in the formulation. Since C30B is characterized
378 by the presence of free hydroxyl groups, the short alkyl chains of the C30B organic

379 modifier would make these groups available for interactions with the polymer
380 macromolecules and HT reactive functional groups, resulting in higher dispersion
381 degree of the nanoclay in the polymer matrix[14]. On the other hand, the basal diffraction
382 around 5.2º in nano-biocomposites XRD patterns may correspond to a fraction
383 characterized by a different alkylammonium chain arrangement in the interlayer space
384 or to a small amount of unmodified C30B[26].
385
386 **Barrier properties.**
387 Barrier to oxygen is one of the main issues in the design of materials for food
388 packaging applications. The high sensitivity of many food products to oxygen
389 degradation, microbial growth stimulated by moisture and aroma retention needed for
390 keeping the food quality requires the improvement in biopolymers barrier properties to
391 gases, vapours and aromas[1]. In general, permeability of a polymer to oxygen or water
392 vapour is dependent on some interrelated factors, including polarity, hydrogen bonding
393 between side chains, molar mass and polydispersity, cross-linking, processing
394 methodology, and crystallinity[33].
395 Results obtained for the oxygen transmission rate per film thickness (*e*), OTR•*e*,
396 for all the studied materials are shown in Table 4. Films containing nanoclay showed a
397 slight decrease in OTR•*e* ($p > 0.05$) due to the nanoclay intercalation into the PCL
398 structure. On the other hand, some increase in OTR•*e* was observed for samples with
399 HT ($p > 0.05$). This effect could be due to the plasticizing effect of HT resulting in the
400 increase in the mobility of PCL chains[34]. A significant improvement in oxygen barrier
401 ($p < 0.05$) was achieved for ternary nano-biocomposites containing C30B and 10 wt%
402 HT, rendering more competitive materials for oxygen sensitive products. This result
403 also suggests that the incorporation of the active additive could promote the

intercalation of the nanofiller into the PCL matrix by improving the dispersion of the nanoclay in the PCL matrix and finally improving oxygen barrier properties. A similar effect was observed in nano-biocomposites based on plasticized PLA containing C30B[23]. This improvement in barrier properties may be explained by the theory developed by Nielsen[35], based on the tortuous pathway that gas molecules should follow to diffuse through the polymer. This tortuosity is produced by the good dispersion in the matrix of the layered silicates platelets, and the consequent longer diffusion pathway increasing the diffusion time and decreasing permeability[33-36]. According to Duncan[35], barrier properties are not only influenced by tortuosity, but also by changes in the polymer matrix at the interfacial regions. In the case of favourable interactions between polymer and nanofiller, polymer strands close to each nanoparticle can be partially immobilized, working against the gases diffusion. In this sense, the Beall[30] model states that the polymer region around the clay affecting diffusion is the constrained region, characterized by lower free volume and diffusion coefficient.

Regarding the nanofiller content, no significant differences were observed by comparing OTR•*e* results for films containing 2.5 and 5 wt% of nanoclay ($p > 0.05$), suggesting a possible filler agglomeration in films with higher amounts of C30B. In this sense, Sánchez et al. found that composites containing 5 wt% of different nanofillers exhibited the highest oxygen barrier performance, and that the addition of larger amounts of nanoclays (10 wt%) to various biopolyesters did not result in further oxygen barrier improvements[1]. These results suggest that there should be a balance between the filler content, the nanocomposite morphology and the possibility of permeability deterioration caused by filler agglomeration[22].

Colorimetric analysis.

Colour is an important factor to be considered for some industrial applications. Colorimetric analysis of films was carried out to evaluate the effect of the presence of the studied additives (Table 4) in this important property. Significant differences in colour were observed as the result of the HT and/or C30B addition to PCL ($p < 0.05$). In this sense, neat PCL showed the highest L^* value, with a significant decrease in the presence of additives; especially for the ternary nano-biocomposites, indicating a significant darkening of these films. ΔE^* values increased in ternary nano-biocomposites. A significant improvement in a* and b* values was also found for these films ($p < 0.05$) resulting in a slightly amber colour. Similar colour changes were reported for polypropylene stabilized with hydroxytyrosol[22], contributing to strengthen the colour of the obtained films. Rhim[37] also reported a decrease in L* values and an increase in b* and ΔE^* values in films produced by blending agar with C20A and C30B, suggesting that differences in colour might be attributed to the dispersion of the nanoclays in the polymer matrix.

Release of HT from PCL nano-biocomposites.

The combination of active additives and nanocomposites can synergistically lead to materials with balanced properties and functionalities for food packaging applications. The formulation of novel antioxidant nano-biocomposites based on PCL and HT can be considered as a way to control solubility and release of the antioxidant agent to foodstuff. In this sense, phenolic compounds from virgin olive oil, such as HT, are known to play an antioxidant role in preventing biomolecules damage. One of the most abundant components of olive oil is an oleuropein derivative named oleacein (dialdehydic form of decarboxymethyl elenolic acid linked to HT)[38]. The evaluation of equilibrium and kinetic properties of hydroxytirosol in these nano-biocomposite films

454 was carried out with methanol as release media. It is known that the tendency of HT
455 (and other phenols) to be solubilized, transferred, or diffused into a given solvent is
456 governed by thermodynamics. One of the primary thermodynamics factors describing
457 this tendency is the activity coefficient[39] which increases as solubility decreases.
458 Although methanol is not commonly used as food simulant, the activity coefficient of
459 HT at 25 ºC in this solvent (0.20) is in-between those shown in ethanol (0.027) and
460 water (0.91)[40] allowing to explore broader applications of these nano-biocomposites.
461 Figure 3a shows the HT release for the three obtained nano-biocomposite films
462 containing HT 10 wt%. As it can be seen, desorption equilibrium was reached after ca. 1
463 hour from the beginning of the process. It is important to note that the release
464 experiment was very aggressive, because materials were completely immersed in
465 methanol. The presence of the nanoclay leads to the decrease in the HT release, with
466 cumulative release values of 7.9 and 7.7 % for C30B2.5 and C30B5, respectively (Table
467 5). This behaviour could be probably related to interactions between C30B and HT. In
468 this sense, Sánchez et al. found an enhancement in thymol solubility in PCL
469 nanocomposites due to the presence of nanoplatelets, possibly due to the retention of the
470 active agent over their surface[1]. They also found a decrease in the thymol diffusion
471 coefficient with the addition of nanoclays, as the result of the tortuous path imposed to
472 the diffusion of the active agent through the nanocomposite bulk. These results suggest
473 that it is possible to control the release of natural agents with interest in the design of
474 novel active films and coatings through incorporation of laminar nanoclays into
475 bioplastics, such as PCL. A similar behaviour was found for Pereira et al. for urea-
476 montmorillonite nanocomposites, showing slower release when compared to pure
477 urea[41]. This profile was probably related to the fact that, as a consequence of some
478 interaction between montmorillonite and urea, this compound would need to adsorb in

479 montmorillonite platelets after its dissolution; also showing the importance of
480 exfoliation in the controlled release.

481 The assessment on the release mechanism was performed by using the power law
482 Korsemeyer-Peppas equation[42]

483 $$C_t/C_\infty = kt^n \qquad (4)$$

484 where C_t and C_∞ are the cumulative concentrations of HT released at time t and at
485 infinite time respectively, and k and n are fitting parameters, giving the later useful
486 information on the release mechanism. The validity of eq. (4) is restricted to $C_t/C_\infty <$
487 0.60[43].

488 Figure 3b shows the fitting of Eq. (4) to the experimental data and the computed
489 fitting parameters are summarized in Table 5. It was observed that the desorption
490 mechanism of HT in PCL/HT10 is non-Fickian ($0.5 < n < 1$), which is indicative of
491 coupling diffusion and relaxation mechanisms. However, for nano-biocomposites n
492 values were approximately 0.5, showing that HT desorption is diffusion-controlled (so-
493 called Fickian). In this case, the apparent diffusion coefficients, D_{ap}, can be computed
494 directly from k, by using the following equation

495 $$k = (4/l)*(D_{ap}/\pi)^{0.5} \qquad (5)$$

496 where l is the film thickness (cm). The calculated diffusion coefficients for HT
497 desorption from PCL/HT10/C30B2.5 and PCL/HT10/C30B5 were 2.9 (± 0.5) × 10^{-10}
498 $cm^2\ s^{-1}$ and 4.5 (± 0.6) × 10^{-10} $cm^2\ s^{-1}$, respectively. These values show that the release
499 of HT under these conditions is very slow and also suggests that the diffusion follows
500 the trend of the O_2 permeation; that is, an increase in the nanoclay content leads to an
501 increase in O_2 permeation and HT diffusion. Taking into account these data, it comes
502 out that the transport mechanism is rather complex and the reasons behind that are not
503 yet well understood.

504

505 **Conclusions**

506 In conclusion, the effect of the addition of HT and C30B on properties of PCL-
507 based nano-biocomposites was evaluated by using several analytical techniques. In this
508 sense, some decrease in elastic modulus was observed for films containing HT,
509 suggesting some plasticizing effect in the polymer matrix. On the other hand, the
510 incorporation of C30B resulted in some decrease in thermal stability and a significant
511 enhancement in oxygen barrier and tensile properties, due to the successful intercalation
512 of the nanofiller into the matrix. Slight differences in colour with the addition of the
513 additives for all films were also observed. Nano-biocomposites showed slow release for
514 HT, which is an important result for its potential application as PCL-based active films
515 and coating systems, with eventual substitution of common synthetic antioxidants used
516 in packaging materials. The obtained PCL-based nanocomposites have shown improved
517 functional properties and can be regarded as potentially interesting materials for active
518 packaging applications within the food manufacturing and agricultural sectors. To
519 complete these investigations, further tests are to be carried out in order to evaluate the
520 migration and antioxidant performance of these nano-biocomposites by contact with
521 food.

522

523 **ACKNOWLEDGEMENTS**

524 Authors would like to thank “Fine & Performance Chemicals Ltd.” and “Perstorp”
525 for kindly providing hydroxytyrosol and PCL, respectively. Financial support by the
526 Spanish Ministry of Economy and Competitiveness (Ref. MAT2011-28468-C02-01)
527 and University of Alicante (UAUSTI12-04) is also acknowledged.

528

REFERENCES

(1) Sánchez, MD; Lagaron, JM. Novel clay-based nanobiocomposites of biopolyesters with synergistic barrier to UV light, gas and vapour. *J. Appl. Polym. Sci*. **2010**, *118*, 188-199.

(2) Ludueña, L; Vázquez, A; Álvarez, A. Effect of lignocellulosic filler type and content on the behavior of polycaprolactone based eco-composites for packaging applications. *Carbohyd. Polym.* **2012**, *87*, 411-421.

(3) Woodruff, MA; Hutmacher, DW. The return of a forgotten polymer: Polycaprolactone in the 21st century. *Prog. Polym. Sci*. **2010**, *35*, 1217-1256.

(4) Labet, M; Thielemans, W. Synthesis of polycaprolactone: A review. *Chem. Soc. Rev.* **2009**, *38*, 3484-3504.

(5) Lee, JE; Kim, KM. Characteristics of Soy Protein Isolate-Montmorillonite Composite Films. *J. Appl. Polym. Sci.* **2010**, *118*, 2257-2263.

(6) Khan, R; Beck, S; Dussault, D; Salmieri, S; Bouchard, J; Lacroix, M. Mechanical and barrier properties of nanocrystalline cellulose reinforced poly(caprolactone) composites: Effect of gamma radiation, *J. Appl. Polym. Sci.*, 2013, 129, 3038-3046.

(7) Martínez-Abad, A.; Sánchez, G.; Fuster, V.; Lagarón, JM.; Ocio, MJ. Antibacterial performance of solvent cast polycaprolactone (PCL) films containing essential oils, Food Control, 2013, 34, 214-220.

(8) Sánchez-García, MD.; Ocio, MJ.; Giménez, E.; Lagaron JM. Novel polycaprolactone nanocomposites containing thymol of interest in antimicrobial film and coating applications. *J Plast. Film Sheet.* **2008**, *24*, 239-251.

(9) Pérez-Masiá, R., López-Rubio, A., Fabra, MJ., Lagarón, JM. Biodegradable polyester-based heat management materials of interest in refrigeration and smart packaging coatings. *J. Appl. Polym. Sci.*, 2013, 130, 3251-3262.

(10) Swapna, JC.; Prashanth, H.; Rastogi, NK.; Indiramma, AR.; Reddy, Y.; Raghavarao, KSMS. Optimum Blend of Chitosan and Poly-(ε-caprolactone) for Fabrication of Films for Food Packaging Applications. 2011 *Food Bioprocess Tech.*, *4*, 1179-1185.

(11) Azeredo, H. Nanocomposites for food packaging applications. *Food Res. Int.* **2009**, *42*, 1240-1253.

(12) Ahmed, J; Auras, R; Kijchavengkul, T; Varshney, SK. Rheological, thermal and structural behavior of poly(ε-caprolactone) and nanoclay blended films. *J. Food Eng.* **2012**, *111*, 580-589.

(13) Oana, MI; Biqiong, C. Porous exfoliated poly(ε-caprolactone)/clay nanocomposites: Preparation, structure, and properties. *J. Appl. Polym. Sci.* **2012**, *125*, 102-112.

(14) Pantoustier, N; Lepoittevin, B; Alexandre, M; Dubois, P; Kubies, D; Calberg, C; Jéröme R. Biodegradable polyester layered silicate nanocomposites based on poly(ε-caprolactone). *Polym. Eng. Sci.* **2002**, *42*, 1928-1937.

(15) Fukushima, K; Tabuani, D; Camino G. Nanocomposites of PLA and PCL based on montmorillonite and sepiolite. *Mat. Sci. Eng.* **2009**, *29*, 1433-1441.

(16) Costantino, U; Bugatti, V; Gorrasi, G; Montanari, F; Nocchetti, M; Tammaro, L; Vittoria V. New polymeric composites based on poly(ε-caprolactone) and layered double hydroxides containing antimicrobial species. *Appl. Mat. Interf.* **2009**, *1,* 668-677.

574 (17) Fabra, M.J; Hambleton, A; Talens, P; Debeaufort, F; Chiralt A. Effect of ferulic
575 acid and α-tocopherol antioxidants on properties of sodium caseinate edible films. *Food*
576 *Hydrocol.* **2011,** *25*, 1441-1447.
577 (18) Abdollahi, M.; Rezaei, M; Farzi G. A novel active bionanocomposite film
578 incorporating rosemary essential oil and nanoclay into chitosan. *J. Food Eng.* **2012**,
579 *111,* 343-350.
580 (19) Salmieri, S.; Lacroix, M. Physicochemical properties of alginate/polycaprolactone-
581 based films containing essential oils. *J. Agric. Food Chem.* **2006**, *54,* 10205-10214.
582 (20) López, A.; Lagaron, JM. Improvement of UV stability and mechanical properties
583 of biopolyesters through the addition of β-carotene. *Polym. Degrad. Stabil.* **2010**, *95,*
584 2162-2168.
585 (21) Bubonja, M.; Giacometti, J.; Abram J. Antioxidant and antilisterial activity of olive
586 oil, cocoa and rosemary extract polyphenols. *Food Chem.* **2011**, *127*, 1821-1827.
587 (22) Peltzer, M.; Jiménez A. Determination of oxidation parameters by DSC for
588 polypropylene stabilized with hydroxytyrosol (3,4-dihydroxy-phenylethanol). *J Therm.*
589 *Anal. Calorim.* **2009**, *96*, 243-248.
590 (23) Martino, VP.; Jiménez, A.; Ruseckaite, RA.; Averous L. Structure and properties
591 of clay nano-biocomposites based on poly(lactic acid) plasticized with polyadipates.
592 *Polym. Adv. Technol.* **2011,** *22*, 2206-2213.
593 (24) ASTM D882-09, 2009. Standard test method for tensile properties of thin plastic
594 sheeting. 468 Annual Book of ASTM Standards. Amer. Soc. for Testing and Materials,
595 Philadelphia, PA.
596 (25) Miltner, HE.; Watzeels, N.; Gotzen, NA.; Goffin, AL.; Duquesne, E.; Benali, S.;
597 Ruelle, B.; Peeterbroeck, S.; Dubois, P.; Goderis, B.; Assche, G.; Rahier, H.; Van Mele

598 B. The effect of nano-sized filler particles on the crystalline-amorphous interphase and
599 thermal properties in polyester nanocomposites. *Polymer*. **2012**, *53*, 1494-1506.
600 (26) Persico, P.; Ambrogi, V.; Carfagna, C.; Cerruti, P.; Ferrocino, I.: Mauriello, G.
601 Nanocomposite polymer films containing carvacrol for antimicrobial active packaging.
602 *Polym. Eng.Sci.* **2009***, 49(7),* 1447-1455.
603 (27) Martino, VP.; Jiménez, A.; Ruseckaite RA. Processing and characterization of
604 poly(lactic acid) films plasticized with commercial polyadipates. *J. Appl. Polym. Sci.*
605 **2009**, *112*, 2010-2018.
606 (28) Rhim, JW.; Park, H.M.; Ha, C.S. Bio-nanocomposites for food packaging
607 applications. *Prog. Polym Sci*. **2013**, *38*, 1629-1652.
608 (29) Jamshidian, M.; Tehrany, EA.; Imran, M.; Akhtar, MJ.; Cleymand, F.; Desobry, S.
609 Structural, mechanical and barrier properties of active PLA–antioxidant films. *J. Food*
610 *Eng.* **2012***, 110*, 380-389.
611 (30) Beall, G.W. New conceptual model for interpreting nanocomposite behavior. In:
612 Pinnavaia, T.J., Beall, G.W. (Eds.), Polymer-Clay Nanocomposites. John Wiley &
613 Sons, Inc., **2000**, New York, USA, pp. 267-279.
614 (31) Quilaqueo-Gutiérrez, M.; Echeverría, I.; Ihl, M.; Bifani, V.; Mauri, AN.
615 Carboxymethylcellulose–montmorillonite nanocomposite films activated with murta
616 (Ugni molinae Turcz) leaves extract. *Carbohyd. Polym.* **2012***, 87* 1495-1502.
617 (32) Ludueña, LN.; Kenny, JM.; Vázquez, A.; Álvarez, VA. Effect of clay organic
618 modifier on the final performance of PCL/clay nanocomposites. *Mat. Sci. Eng. A*. **2011**,
619 *529*, 215-223.
620 (33) Duncan, TV. Applications of nanotechnology in food packaging and food safety:
621 barrier materials, antimicrobials and sensors. *J. Colloid Interface Sci.* **2011***, 363*, 1-24.

622 (34) Sothornvit, R.; Krochta JM. Oxygen permeability and mechanical properties of
623 films from hydrolyzed whey protein. *J. Agric. Food Chem.* **2000**, *48*, 3913-3916.
624 (35) Nielsen, LE. Models for the permeability of filled polymer systems. *J. Macromol.*
625 *Sci. A.* **1967**, *1*, 929-942.
626 (36) Molinaro, S.; Romero, MC.; Boaro, M.; Sensidoni, A.; Lagazio, C.; Morris, M.;
627 Kerry J. Effect of nanoclay-type and PLA optical purity on the characteristics of PLA-
628 based nanocomposite films. *J. Food Eng.* **2013***, 117*, 113-123.
629 (37) Rhim, JW.; Lee, SB.; Hong, S.I. Preparation and characterization of agar/clay
630 nanocomposite films: the effect of clay type. *J. Food Sci.* **2011**, *76 (3*), 40-48.
631 (38) Czerwinska, M.; Kiss, AK.; Naruszewicz M. A comparison of antioxidant
632 activities of oleuropein and its dialdehydic derivative from olive oil, oleacein. *Food*
633 *Chem.* ***2012,*** *131*, 940-947.
634 (39) Queimada, AJ.; Mota, FL.; Pinho, SP.; Macedo, EA. Solubility of Biologically
635 Active Phenolic Compounds: Measurements and Modelling, *J Phys Chem B*, **2009**, *113*,
636 3469-3476
637 (40) Galanakis, CM.; Goulas, V.; Tsakona, S.; Manganaris, GA.; Gekas V. A
638 Knowledge base for the recovery of natural phenols with different solvents. *Int. J. Food*
639 *Prop.* **2013**, *16*, 382-396.
640 (41) Pereira, EI.; Minussi, FB.; Da Cruz, CCT.; Bernardi, ACC.; Ribeiro C. Urea-
641 Montmorillonite-Extruded Nanocomposites: A Novel Slow-Release Material. *J. Agric.*
642 *Food Chem.* **2012***, 60*, 5267-5272.
643 (42) Korsmeyer, R.W.; Gurny, R.; Docler, E.; Buri, P.; Peppas, N. A. Mechanisms of
644 solute release from porous hydrophilic polymers *Int. J. Pharm.* ***1983****, 15*, 25-35.
645 (43) Crank, J. The Mathematics of Diffusion 2nd Ed., 1975, Oxford University Press
646 Inc., New York.

FIGURE CAPTIONS

Figure 1. TEM images of neat PCL (A) and PCL/HT5/C30B2.5 (B) nano-biocomposite.

Figure 2. XRD patterns of C30B, PCL, and the obtained PCL bio-nanocomposites in the (2-10º) angle range.

Figure 3. (a) Desorption release profiles (a) and short-time range (C_t/C_∞<0.6) desorption kinetics (b) of HT from PCL/HT10 (□), PCL/HT10/C30B2.5 (o) and PCL/HT10/C30B5 (△) films; solid lines (b) represent the fitting of Eq.(4) to desorption kinetic experimental data.

TABLES

Table 1. PCL nano-biocomposites and thickness (mean ± SD, n = 5).

Table 2. DSC results obtained for all formulations in nitrogen atmosphere (mean ± SD, n = 3). Different superscripts within the same column indicate statistically significant different values ($p < 0.05$).

Table 3. Thermal (mean ± SD, n = 3) and mechanical properties (mean ± SD, n = 5) of the studied films. Different superscripts within the same column indicate statistically significant different values ($p < 0.05$).

Table 4. Colour coordinates (mean ± SD, n=5) and OTR·e values from active films (e: thickness, mm; mean ± SD, n=3). Different superscripts within the same column indicate statistically significant different values ($p < 0.05$).

Table 5. Concentration of HT released in the HT 10 wt% formulations.

Table 1.

Formulation	HT (wt %)	C30B (wt %)	Thickness (μm)
PCL0	-	-	204 ± 3
PCL/HT5	5	-	202 ± 6
PCL/HT10	10	-	206 ± 6
PCL/C30B2.5	-	2.5	191 ± 4
PCL/C30B5	-	5	198 ± 3
PCL/HT5/C30B2.5	5	2.5	196 ± 5
PCL/HT10/C30B2.5	10	2.5	201 ± 3
PCL/HT5/C30B5	5	5	191 ± 2
PCL/HT10/C30B5	10	5	198 ± 4

Table 2.

Sample	T_C (°C)	T_m (°C)	ΔH_C (J g^{-1})	ΔH_m (J g^{-1})	χ (%)
PCL0	28 ± 2^{a}	51 ± 2^{a}	48 ± 1^{a}	66 ± 4^{a}	46 ± 1^{a}
PCL/HT5	32 ± 2^{ab}	56 ± 1^{b}	53 ± 3^{b}	70 ± 2^{a}	49 ± 1^{b}
PCL/HT10	27 ± 3^{a}	55 ± 2^{ab}	55 ± 1^{b}	72 ± 2^{a}	51 ± 2^{b}
PCL/C30B2.5	35 ± 1^{b}	59 ± 2^{b}	58 ± 3^{b}	72 ± 1^{a}	52 ± 2^{b}
PCL/C30B5	34 ± 4^{ab}	58 ± 1^{b}	53 ± 2^{b}	69 ± 2^{a}	51 ± 1^{b}
PCL/HT5/C30B2.5	31 ± 1^{a}	57 ± 3^{b}	52 ± 1^{b}	69 ± 3^{a}	50 ± 1^{b}
PCL/HT10/C30B2.5	28 ± 2^{a}	56 ± 1^{b}	49 ± 2^{ab}	71 ± 2^{a}	51 ± 2^{b}
PCL/HT5/C30B5	28 ± 2^{a}	56 ± 2^{b}	51 ± 2^{ab}	63 ± 2^{a}	47 ± 2^{b}
PCL/HT10/C30B5	27 ± 3^{a}	55 ± 1^{a}	49 ± 1^{ab}	60 ± 4^{a}	48 ± 1^{b}

Table 3

Sample	$T_{ini5wt\%}$ (ºC)	T_{max} (ºC)	ε_B (%)	*E* (MPa)	TS (MPa)
PCL0	348 ± 2^{a}	415 ± 3^{a}	20 ± 1^{a}	507 ± 21^{a}	12 ± 2^{a}
PCL/HT5	350 ± 2^{a}	412 ± 4^{a}	29 ± 2^{b}	453 ± 25^{b}	10 ± 2^{ab}
PCL/HT10	330 ± 3^{b}	416 ± 1^{a}	38 ± 2^{c}	413 ± 25^{b}	10 ± 1^{a}
PCL/C30B2.5	300 ± 5^{c}	409 ± 4^{a}	40 ± 2^{c}	687 ± 31^{c}	9 ± 1^{a}
PCL/C30B5	280 ± 3^{d}	390 ± 2^{b}	49 ± 1^{d}	794 ± 24^{d}	7 ± 1^{b}
PCL/HT5/C30B2.5	330 ± 1^{b}	405 ± 4^{a}	36 ± 3^{c}	491 ± 33^{a}	9 ± 1^{ab}
PCL/HT10/C30B2.5	330 ± 3^{b}	411 ± 1^{a}	41 ± 2^{cef}	463 ± 18^{b}	8 ± 2^{ab}
PCL/HT5/C30B5	328 ± 3^{b}	403 ± 3^{a}	43 ± 2^{e}	622 ± 29^{c}	9 ± 2^{ab}
PCL/HT10/C30B5	327 ± 4^{b}	407 ± 3^{a}	46 ± 1^{ef}	732 ± 45^{d}	7 ± 3^{ab}

Table 4.

Sample	OTR·*e* (cm^3 mm m^{-2} day)	Colorimetric parameters			
		L*	***a****	***b****	ΔE
PCL0	51± 2^{a}	83.6 ± 0.6^{a}	-0.9 ± 0.4^{a}	2.4± 0.6^{a}	-
PCL/HT5	54± 1^{a}	79.1 ± 1.2^{b}	-0.6 ± 0.6^{a}	6.1 ± 0.3^{b}	2.5± 0.2^{a}
PCL/HT10	56 ± 3^{a}	75.5 ± 1.7^{c}	-0.7 ± 0.2^{a}	9.8 ± 0.3^{c}	3.1 ± 0.1^{b}
PCL/C30B2.5	49 ± 4^{a}	76.0 ± 2.2^{c}	-0.9 ± 0.2^{a}	4.1± 0.2^{d}	2.1 ± 0.2^{a}
PCL/C30B5	49 ± 5^{a}	75.4 ± 1.2^{c}	-1.3 ± 0.5^{a}	6.9± 0.4^{b}	2.6 ± 0.2^{a}
PCL/HT5/C30B2.5	50 ± 4^{a}	52.9 ± 0.8^{d}	2.3 ± 0.2^{b}	10.4 ± 0.4^{c}	3.2 ± 0.2^{bc}
PCL/HT10/C30B2.5	31±1^{b}	51.6± 2.9^{d}	3.6 ± 0.8^{c}	12.9 ± 04^{e}	3.6 ±0.3^{c}
PCL/HT5/C30B5	40 ± 3^{c}	47.5 ± 0.9^{e}	3.1 ± 0.6^{c}	11.9 ± 0.6^{e}	3.4 ±0.2^{bc}
PCL/HT10/C30B5	32 ± 2^{b}	40.6 ± 2.8^{f}	2.9 ±0.5^{c}	10.1 ± 0.3^{c}	3.2 ±0.2^{bc}

Table 5

Sample	HT released (%)	Eq. (4)		
		n	***k* / s^{-n}**	**R^2**
PCL/HT10	9.2	0.65 (±0.02)	0.008 (±0.001)	0.9942
PCL/HT10/C30B2.5	7.9	0.56 (±0.01)	0.013 (±0.001)	0.9952
PCL/HT10/C30B5	7.7	0.57 (±0.02)	0.016 (±0.002)	0.9914

R^2: correlation coefficient.

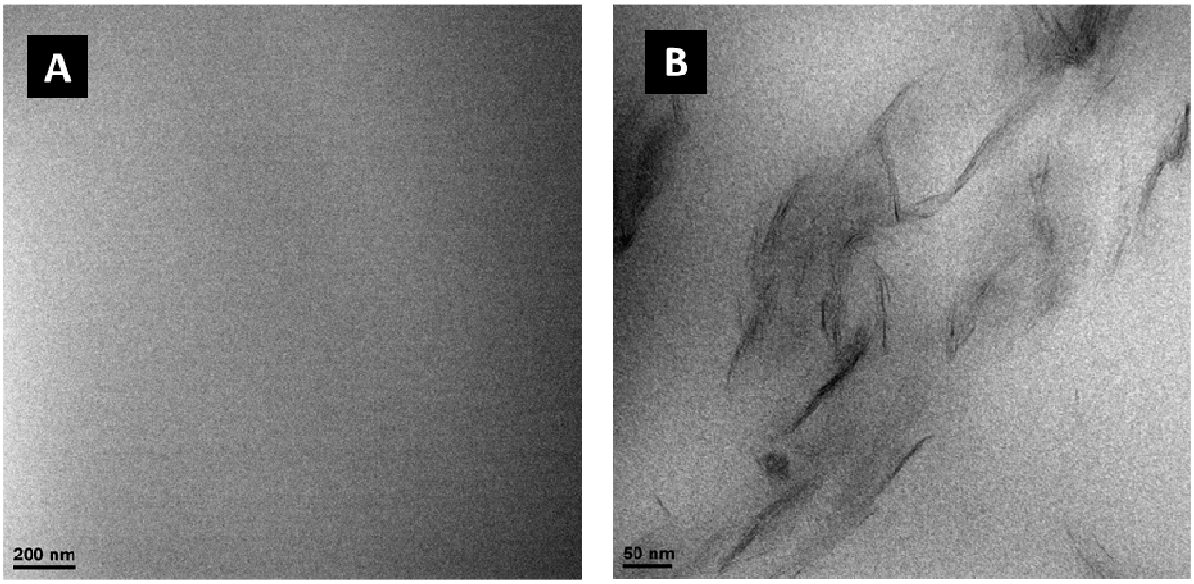

Figure 1.

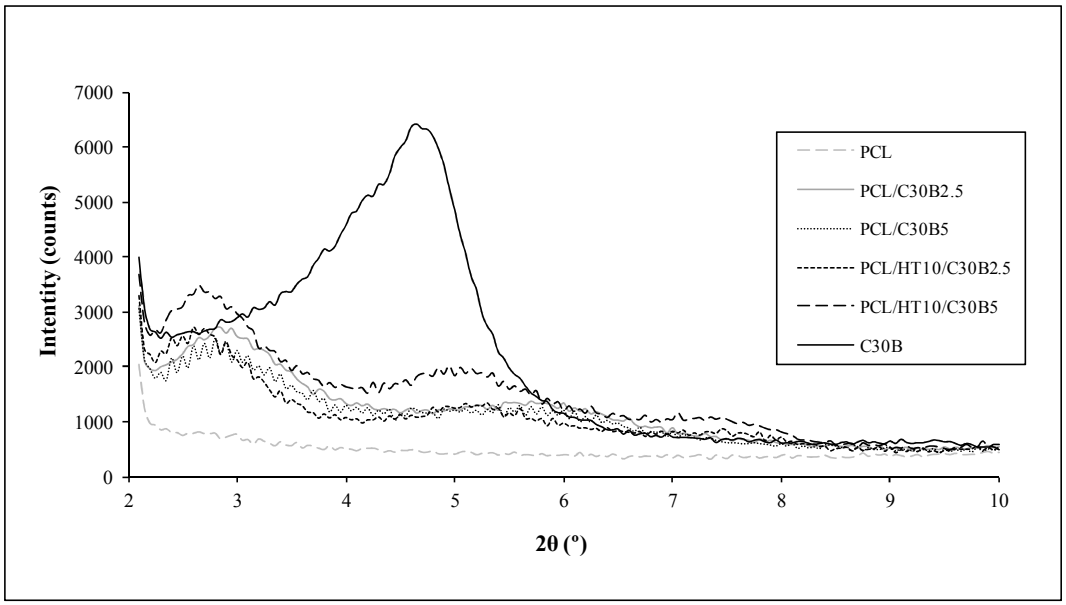
7000
6000
5000
4000
3000
2000
1000
0
Intentity (counts)
2
3
4
5
6
7
8
9
10
2θ (°)
PCL
PCL/C30B2.5
PCL/C30B5
PCL/HT10/C30B2.5
PCL/HT10/C30B5
C30B

Figure 2.

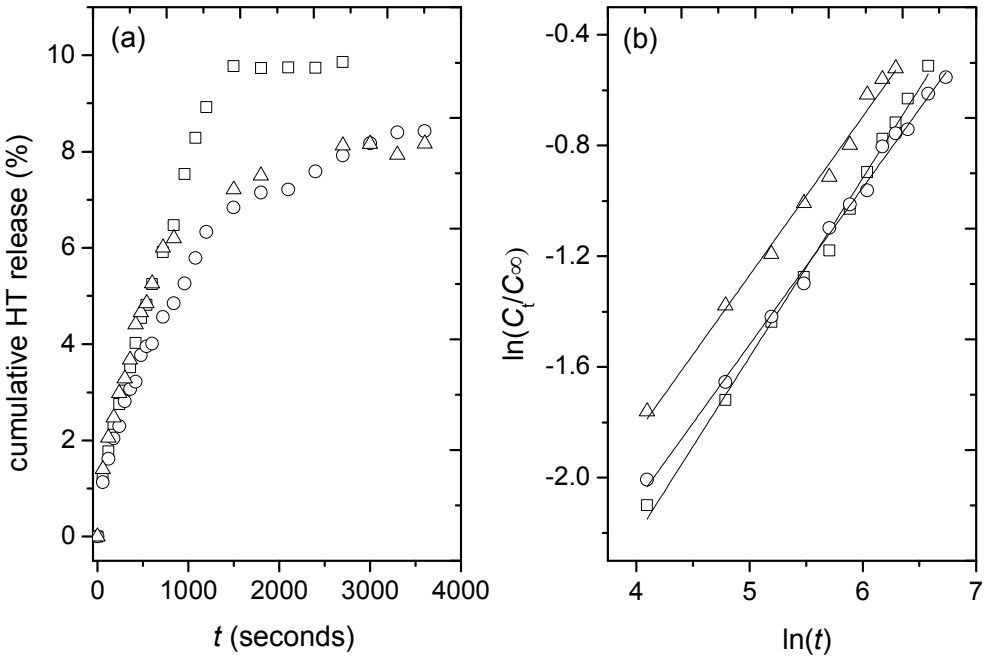
(a)
cumulative HT release (%)
t (seconds)
0
2
4
6
8
10
0
1000
2000
3000
4000
(b)
ln(Ct/C∞)
ln(t)
-0.4
-0.8
-1.2
-1.6
-2.0
4
5
6
7

Figure 3.

TOC Graphic

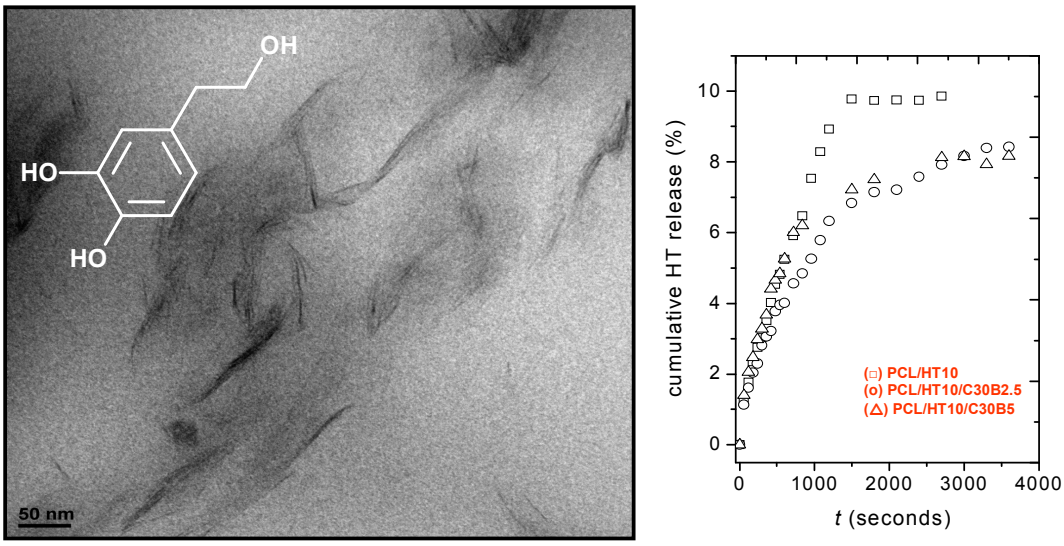
OH
HO
HO
50 nm
cumulative HT release (%)
t (seconds)
(□) PCL/HT10
(o) PCL/HT10/C30B2.5
(△) PCL/HT10/C30B5
0
2
4
6
8
10
0
1000
2000
3000
4000